# Performance Analysis of a Power-to-Gas Storage System based on r-SOC



Journal of Physics: Conference Series **2893** (2024) 012051 doi:10.1088/1742-6596/2893/1/012051

# Performance Analysis of a Power-to-Gas Storage System based on r-SOC

**M A Ancona[1], G Brunaccini[2], A De Pascale[1], F Ferrari[1], M Ferraro[2], C Italiano[2], T Santangelo[3*], A Vita[2]**

[1] Department of Industrial Engineering (DIN), University of Bologna, Bologna, Italy
[2] Institute of Advanced Energy Technology (ITAE), National Research Council (CNR), Messina, Italy
[3] Inter-Departmental Center for Industrial Research on Renewable Sources, Environment, Sea and Energy (CIRI-FRAME), University of Bologna, Bologna, Italy

[*]E-mail: tania.santangelo2@unibo.it

**Abstract.** Power-To-Power (P2P) systems represent a promising technology to store the overgeneration from renewables generating a synthetic gas (mostly hydrogen or methane) and to convert the chemical carrier back into electricity during periods of energy demand peaks. In this context, the aim of this work is to propose, model and analyse an innovative P2P system that includes, as key components, a reversible Solid Oxide Cell (r-SOC) device and a reversible chemical reactor (RCR) working both as methanator and reformer. In the synthetic fuel production phase, water and electricity are converted into hydrogen by the r-SOC, which operates as an electrolyzer. Then, the hydrogen is in turn converted into synthetic methane by the RCR, operating as a methanator. During the discharge phase, instead, the RCR device operates as a reformer, fed by methane and water, and the r-SOC operates as a fuel cell, feeding the electricity production into the grid. The whole reversible P2P is modelled in Aspen HYSYS environment allowing to simulate both the design and off-design operation of the system. In addition, to increase the whole system's performance, a heat recovery section is included in the model and optimized. Finally, a preliminary analysis to reproduce the behaviour of the system on varying the input available electric power will be analyzed and discussed, introducing and evaluating the key performance parameters for the system.

## 1. Introduction

The current issues related to traditional fuels show how it is necessary to move beyond this era. Renewable Energy Sources (RES) seem to offer a solution to reduce the use of fossil fuels [1], but their non-programmability and difficult coupling with energy storage systems pose various issues [2]. In this context, power-to-power systems offer the possibility of storing the electricity surplus from renewables within a green fuel, to be reconverted in periods of high energy demand and/or low availability of the RES. Particular interest is indeed being posed in hydrogen and methane energy storage, since it is demonstrated that power-to-gas systems can accumulate a higher amount of energy compared to simple battery storage [3].

In general, the synthetic natural gas (SNG) produced by the system in Power-To-Gas (P2G) mode can envisage several uses: it can be stored for later reconversion in the Gas-To-Power (G2P)

phase or – after a proper conditioning process – it can be fed into the natural gas grid, or again used in the automotive sector, in natural gas-powered vehicles [4]. The process of producing SNG involves using $CO_2$, which can be injected into the Power-to-Gas (P2G) system either during the high-temperature electrolysis phase (co-electrolysis) or as an input to the methanation section. The $CO_2$ needed for SNG production can be obtained from Carbon Capture and Storage (CCS) systems [5]. The topic is currently widely studied in the literature: as an example, Paulina Pianko-Oprych et al. [6] investigate a G2P system comprising a reformer and a Solid Oxide Fuel Cell (SOFC), while Maximilian Hauck et al. [7] analyze a Power-To-Power (P2P) system centered around an r-SOC. Other studies, such as that of Bin Chen et al. [8], consider a combined system that couples the reversible solid oxide device with $CO_2$ methanation for grid stabilization.

As innovative step compared to the current available literature, the aim of this work is to propose and study a new P2P system (see Figure 1) consisting of two reversible devices: r-SOC (reversible Solid Oxide Cell) and RCR (reversible chemical reactor). These reversible devices, according to the operational mode, can work as: i) SOEC (Solid Oxide Electrolyzer Cell) and methanator, in the storage (charge) phase; ii) reformer and SOFC (Solid Oxide Fuel Cell), in the restitution (discharge) phase. In addition, in the production phase, the SNG at the outlet of the RCR is fed to a further methanation section (named here as mid-temperature methanation, operating at a lower temperature than the RCR, corresponding to conventional methanation conditions), to allow methane enrichment, and to a conditioning section, to achieve the opportune composition and pressure for the introduction into the natural gas network.

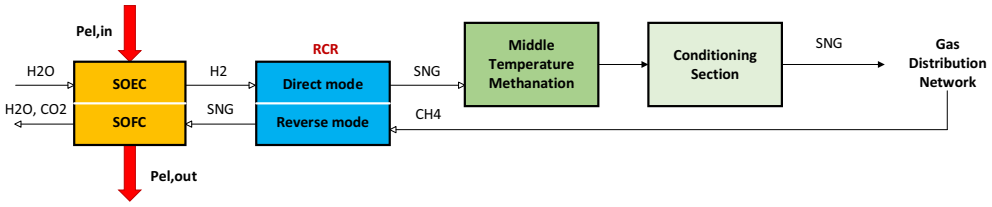


**Figure 1.** Simplified schematic of the proposed P2P system based on the two key reversible devices (r-SOC and RCR).

## 2. Thermodynamic model and assumptions

The general scheme of the P2P storage system operating modes investigated in this work is presented in the block diagram of Figure 2, where A denotes the charge phase (i.e., the synthetic fuel production phase), and B represents the discharge phase (i.e., the reconversion of the SNG into electricity).

The production phase is realized by three main sections: (*i*) the Solid Oxide device operating as SOEC, fed by water and renewable electricity, (*ii*) a high-temperature methanation section fed by the SOEC cathode outlet and by a $CO_2$-rich gas stream, and (iii) a middle-temperature methanation section. Furthermore, an internal hydrogen recirculation stream is typically accounted to improve the SOEC performance (see, for example, Giglio et al. [4]). The downstream SNG conditioning section, analyzed in a previous study [9], is not proposed here for the sake of brevity. On the other hand, the discharge phase includes: (*i*) the reformer section, fed by a fuel stream (e.g, the $CH_4$-rich stream produced in the charging mode) and by water, and (*ii*) the Solid Oxide device operating as Fuel Cell (SOFC), which is fed by the reformer outlet syngas and by air.

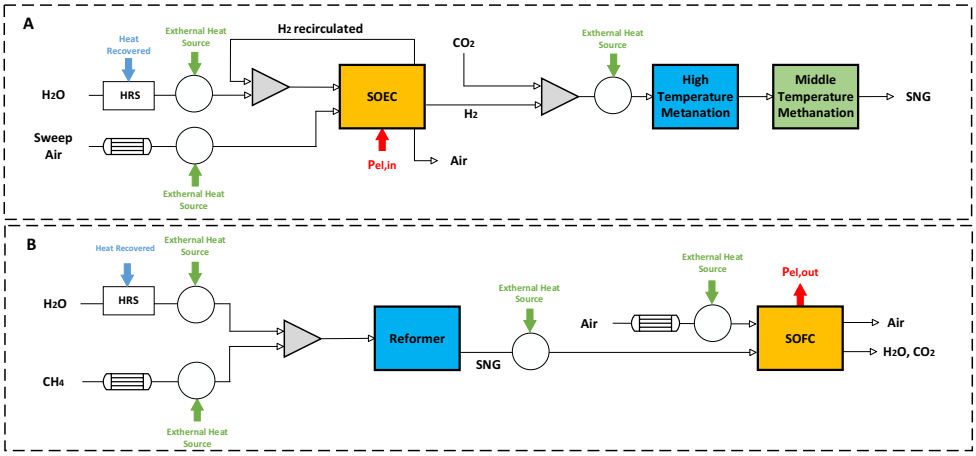


**Figure 2.** P2P system operating modes schematics: charge phase (A) and discharge phase (B).

The main material streams and power input/output contributions are highlighted in the figure. A lumped-parameter thermodynamic model of the system has been implemented in ASPEN HYSYS™ environment [10] in order to simulate the entire energy system in both modes. In the following paragraphs, the main assumptions adopted to reproduce each subsection of the system are presented. The model has been calibrated using specific data from experimental small-scale prototypes of the components, tested within the CNR-ITAE laboratory.

*2.1 Charge phase modelling*

Figure 3 shows the model layout implemented in the software graphical interface to reproduce the system in the SNG production phase (P2G).

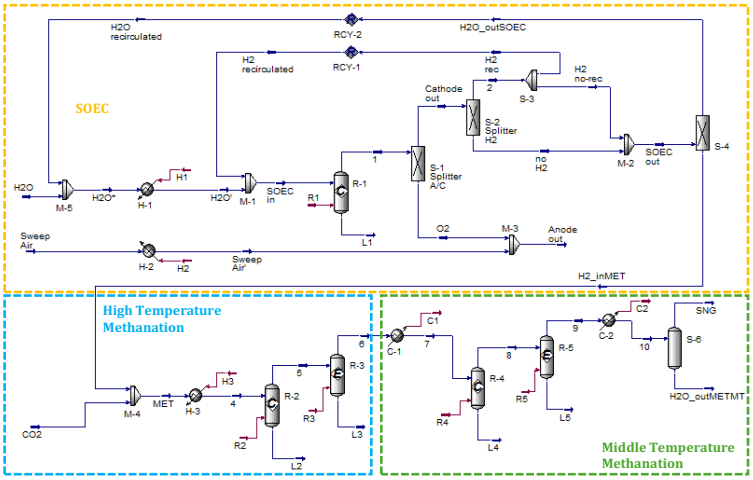


**Figure 3.** Aspen Layout of P2G mode.

The key sections of the system configuration and the related operating ranges are: (i) the high-temperature SOEC (700-950 °C [11]); (ii) the high-temperature methanation section (500-650

°C); (iii) the middle-temperature methanation (350-450 °C). Heaters and/or coolers between the main components are required due to different thermal levels, as detailed in the following sections.

*2.1.1 Solid Oxide Electrolyzer Cell section*

The electrolyzer has been simulated in Aspen HYSYS™ by the use of standard components of its library (namely by integrating reactors, separators, splitters and mixers). In detail, the SOEC functionalities are modelled mainly with a conversion reactor (*R-1*), three separators (*S-1*, *S-2*, and *S-4*), and a splitter (*S-3*). The reactor *R-1*, where the electrolysis reaction (1) occurs:

$$H_2O \rightarrow H_2 + 0.5\, O_2 \quad (1)$$

is fed with water and with a recirculated stream of hydrogen and residual water. At the outlet of the electrolysis reactor, the physical separation of the anodic ($O_2$-rich) and cathodic ($H_2$, $H_2O$) outlet streams is modelled by the separator (*S-1 Splitter A/C*). At the outlet of the cathodic compartment, the *S-2* separator of hydrogen and splitter *S-3* are used in order to model the hydrogen recirculation stream. While, the S-4 splitter is used to simulate the removal of residual water from the produced hydrogen stream, which is then recirculated and injected upstream along with the electrolyzer feedwater.

The SOEC anodic compartment has been modelled including the sweep air stream, which is mixed with the oxygen produced by the reaction. The conversion reactor rate is set to 86% and the $H_2$ recirculation rate is set to 11% to prevent cathode deactivation [12].

Reactant flow rates are set to achieve a reference SOEC electric input power. a further assumption in this study is to consider the design point of the SOEC coincident with the thermoneutral condition, i.e., the electrochemical process is at its thermodynamic equilibrium. Moreover, the same temperature value is set for both inlet reactants and products of the SOEC, i.e., isothermal conditions [13].

The anode (*Sweep Air*) and the cathode (*H2O*) inlet streams are heated up to the operating temperature of the SOEC (700 °C) through heaters *H-2* and *H-1*, respectively. The sweep air flow rate is set to have a ratio of the molar flow rate of oxygen produced to oxygen leaving the anode section equal to 11%.

*2.1.2 Reversible chemical reactor section and middle-temperature methanation section*

The RCR operating as a high-temperature methanator (production phase) aims at reproducing the experimental reactor installed at the CNR test bench, which is a tubular catalytic bed reactor Incoloy® 800HT (inner diameter 21 mm, outer diameter 22 mm, length 200 mm) with a structured ceramic foam catalyst (25 %wt Nickel/Cerium-Zirconium - Ni/CeZr - diameter 20 mm, length 150 mm). Furthermore, the reactor is air-cooled to remove the reaction heat that circulates inside the reactor shell, both counter-current and co-current [14].

The methanation process is modeled in Aspen HYSYS™ using standard blocks from the software library tuned with experimental data. In detail, at the inlet of the high-temperature methanation section, the SOEC cathode outlet, stripped of water vapor (by the *S-4* component), is mixed (in *M-4*) with $CO_2$ and heated (via *H-3*) to the RCR operating temperature. The $CO_2$ inlet flow rate is adjusted to set the $H_2$:$CO_2$ ratio equal to 4:1.

The RCR section in charge mode is modelled by means of two reactors, namely a conversion reactor (*R-2*), for the conversion of $CO_2$ in $CH_4$ (2), and an equilibrium reactor (*R-3*), for the Reverse Water-Gas-Shift reaction (RWGS) (3):

$$CO_2 + 4H_2 \rightarrow CH_4 + 2H_2O \quad (2)$$
$$CO_2 + H_2 \rightarrow H_2O + CO \quad (3)$$

The middle-temperature methanator, modeled with the same blocks structure of the high-temperature methanator, includes also the CO methanation reaction (4):

$$CO + 3H_2 \rightarrow CH_4 + H_2O \quad (4)$$

The RCR outlet stream undergoes cooling (*C-1*) to the operating temperature of the middle-temperature section. Eventually, the methanation output stream is cooled in *C-2* to 25°C.The conversion rate (*CR*) of the methanation reactions in *R-2* and *R-4* was modelled as a function of the operating temperature via a second-order polynomial equation (5), reported in Figure 4:

$$CR = C_0 + C_1 \cdot T + C_2 \cdot T^2 \quad (5)$$

where, $T$ [K] is the mean operating temperature of the reactor, and $C_0$, $C_1$, and $C_2$ are the tuned coefficients of the interpolating function. The second-order polynomial interpolation was found to match experimental data collected with tests on the RCR performed at the CNR laboratories in different operating ranges of inlet conditions, as shown in Figure 4.

In particular, the two sets of curves refer to two experimental tests on the same methanation reactor, in which the mean temperature was observed respectively in the ranges 350-500°C and 550-600°C. The coefficients of the interpolating function in the range of reactors *R-2* and *R-4*, respectively, are: $C_0$ = -957.4071; $C_1$ = 2.5132; $C_2$ = -0.0015; $C_0$ = -243.0554; $C_1$ = 0.8899; $C_2$ = -6.2158e$^{-4}$.

Finally, the boundary conditions and assumptions made for the P2G system are presented in Table 1.

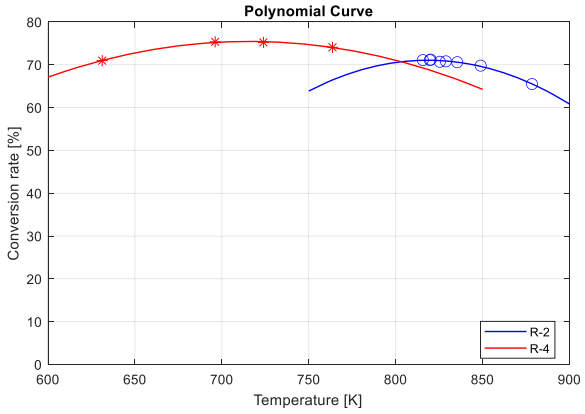


**Figure 4.** Experimental CR data for methanation and polynomial interpolation in the *R-2* and *R-4* ranges.

**Table 1.** P2G system boundary conditions and assumptions.

| | Parameter | Value | Units |
|---|---|---|---|
| Electrolyzer | Inlet $H_2O$ stream temperature | 25 | °C |
| | Inlet $H_2O$ stream pressure | 100 | kPa |
| | Operating temperature | 700 | °C |
| | Operating pressure | 100 | kPa |
| | Input power | 3.60 | kW |
| | Inlet $H_2O$ flow rate | 0.95 | kg/h |
| | Conversion efficiency | 86 | % |
| | Inlet Sweep Air temperature | 25 | °C |
| | Inlet Sweep Air pressure | 100 | kPa |
| | $O_2$ molar fraction at anodic outlet | 0.23 | - |
| | $H_2$ molar fraction at SOEC reactor inlet | 11 | % |
| High Temperature Methanation | Experimental reactor temperature range | 500-650 | °C |
| | Experimental reactor operating pressure | 100 | kPa |
| | $H_2$ /$CO_2$ molar ratio | 4 | - |
| | Inlet $CO_2$ stream temperature | 25 | °C |
| Middle Temperature Methanation | Experimental reactor temperature range | 350-450 | °C |
| | Experimental reactor operating pressure | 100 | kPa |

*2.2 Discharge phase modeling*

The system discharge phase configuration is shown in Figure 5. The considered reformer temperature range is 600-700 °C, while the downstream SOFC temperature is considered equal to the SOEC operating temperature [15].

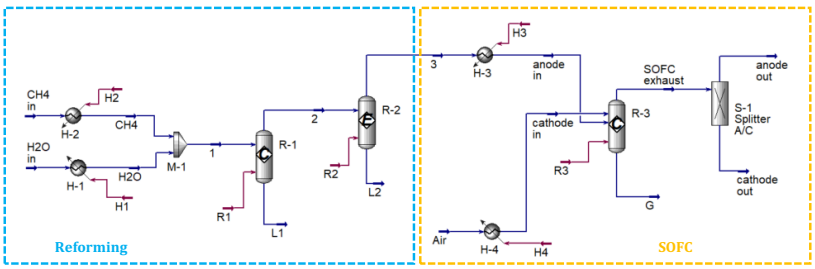


**Figure 5.** Aspen Layout of G2P mode.

*2.2.1 Reversible chemical reactor*

In the discharging phase operation, the RCR (working as a reformer) is fed with $CH_4$ and $H_2O$ in order to ensure a Steam-to-Carbon ratio (S/C) equal to 3. The inlet $CH_4$ flow rate has been set in the model to match the downstream SOFC design power.

Water and methane streams are heated in *H-1* and *H-2*, respectively, and then mixed to enter the conversion reactor (*R-1*) which simulates the reforming of $CH_4$ into $H_2$ and CO (6). In addition, an equilibrium reactor (*R-2*) is used to simulate the Water Gas Shift (WGS) reaction (7):

$$CH_4 + H_2O \rightarrow CO + 3H_2 \quad (6)$$
$$CO + H_2O \rightarrow CO_2 + H_2 \quad (7)$$

Experimental values of the RCR conversion rate provided by the CNR test bench operated in reverse mode at 600 °C and 700 °C, with pressure equal to 100 kPa, are used to tune the model. A comparison between the experimental and simulation points in terms of outlet composition is reported in Figure 6. The figure shows very similar experimental and simulation values, especially for $CH_4$, CO and $CO_2$, while the $H_2$ and $H_2O$ values show a slightly larger error (slight overproduction of $H_2$, with a 10% error at 600°C and a 6% error at 700°C).

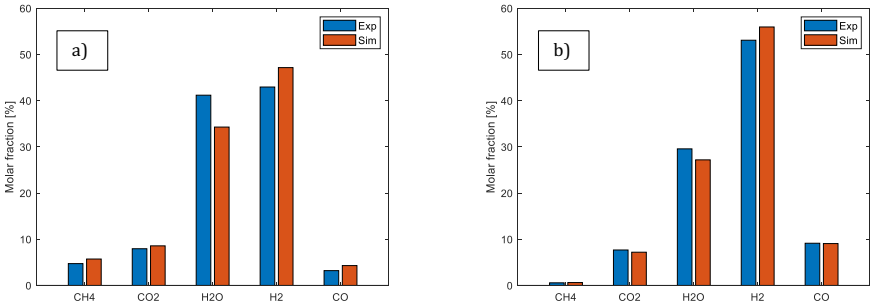


**Figure 6.** Experimental and simulated outlet mass fractions of RCR (reformer mode) at ambient pressure and two operating temperature values: a) 600 °C and b) 700 °C.

*2.2.2 Solid Oxide Fuel Cell section*

The RCR outlet stream is heated in *H-3* and sent to the SOFC as inlet anodic stream. The cathodic stream is air, preheated (with *H-4*) at the same temperature as the cell (700°C). Moreover, the same temperature value is set for both inlet reactants and products of the SOFC, i.e., isothermal conditions.

As for the SOEC section, the developed model uses standard components from the library to simulate the SOFC. In detail, the cell has been simulated as a conversion reactor (*R-3* in Figure 5) where the oxidation reactions of $H_2$ (8) and CO (9) occurs:

$$H_2 + 0.5\, O_2 \rightarrow H_2O \quad (8)$$
$$CO + 0.5\, O_2 \rightarrow CO_2 \quad (9)$$

Physical separation between products takes place thanks to a component splitter (S-1 Splitter A/C) to model the anode and the cathode outlet stream separation. Table 2 summarizes the main input parameters of the G2P system. In addition, the flow rate of air injected into the SOFC (*Air* Figure 5) is adjusted according to the hydrogen present in the anode current (*anode in*), and the Air/$H_2$ ratio is kept constant and equal to 9, in line with the manufacturer data.

**Table 2.** G2P system boundary conditions and assumptions.

| | Parameter | Value | Units |
|---|---|---|---|
| Reformer | Inlet $H_2O$ stream temperature | 25 | °C |
| | Inlet $H_2O$ stream pressure | 100 | kPa |
| | Inlet $CH_4$ stream temperature | 25 | °C |
| | Inlet $CH_4$ stream pressure | 100 | kPa |
| | $CH_4$ flow | 0.19 | kg/h |
| | Experimental reactor temperature range | 600-700 | °C |
| | Experimental reactor operating pressure | 100 | kPa |
| | Conversion efficiency (at 600°C) | 69 | % |
| | Conversion efficiency (at 700°C) | 96 | % |
| | S/C | 3 | - |
| Fuel cell | Operating temperature | 700 | °C |
| | Operating pressure | 100 | kPa |
| | Electric output power | 1.20 | kW |
| | Fuel Utilization factor | 0.80 | - |
| | Air/$H_2$ molar ratio | 9 | - |
| | Air in temperature (before preheating) | 25 | °C |
| | Air in pressure | 100 | kPa |

*2.3 Heat recovery*

The configuration described above is not thermally efficient, since the P2P system requires a certain amount of thermal energy to heat the incoming streams for both the charge and discharge phases, while cooling is required in other sections of the integrated system.

As a consequence, the model previously presented has been improved by introducing a heat recovery section with an optimized configuration based on the optimal operating temperature levels of the components. Namely, the high-temperature methanation section is set at 550°C, the middle-temperature methanation section at 450°C, and the reformer at 600°C. The latter temperature is chosen so that the RCR operates at approximately the same temperature.

*2.3.1 Charge phase*

The temperature of the reactant entering the SOEC (*H2O*) must be increased from the ambient temperature up to the operating temperature of the SOEC, thus a high thermal input is required.

In order to limit the external heat demand and to preheat the inlet water, heat exchangers are introduced to recover – where it is possible – the hot streams coming out from the following sections of the integrated system. The system configuration, including the heat recovery section for the direct mode operation, is shown in Figure 7.

Three heat exchangers are introduced in the Heat Recovery Section (HRS) to preheat water at the cathode inlet, and another heat exchanger is used to preheat air at the anode inlet.

The hot stream of the SOEC anode outlet (*out*) is used for preheating the *Sweep Air* current (in *HX-1*). A first heat exchanger on the water line (*HX-2*) is used to evaporate water with the residual heat content of the hot gas stream discharged by *HX-1*. A second heat exchanger (*HX-3*) allows heat recovery from the outlet stream of the middle-temperature methanation section (stream *9*). A further heat exchanger in the water preheating line (*HX-4*) is used to recover heat from the cathode outlet of the SOEC up to 500°C.

In addition, to consider external heat supply when the HRS is not sufficient to heat the SOEC inlet streams, the heaters *H-1* (in the water line) and *H-2* (in the *Sweep Air* stream) are included.

The heat exchanger *HX-5* is used to preheat the inlet $CO_2$ by taking advantage of the high-temperature methanation outlet stream. In addition, a heater (*H-3*) allows to meet the operating temperature of the second step of methanation. An optional external cooler (*C-1*) is also included in Figure 3 to regulate the methanation at different temperature conditions. The final cooler *C-2* is used to cool at ambient temperature and to separate the produced SNG stream from residual water.

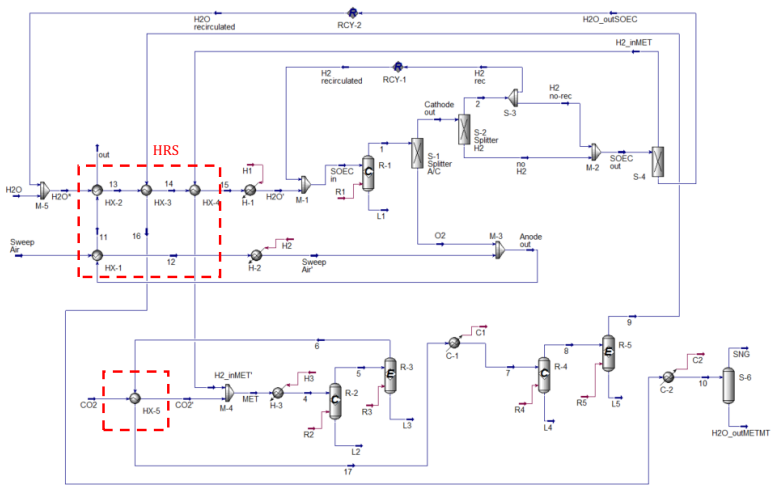


**Figure 7.** Heat recovery arrangement in the P2G mode.

*2.3.2 Discharge phase*

In the discharge phase, an internal heat recovery section (HRS) has been included to preheat the reformer reactants, as illustrated in Figure 8. The two external heaters (*H-1* and *H-2*) are also included. Preheating takes place in the HRS through two heat exchangers along the feedwater line and one along the methane line.

Water is preheated in *HX-1*, which allows water vaporization by using the SOFC cathode outlet, and in *HX-2*, fed by the current coming out of the *HX-3* exchanger. Methane is preheated with the *HX-3* exchanger, which is fed by the SOFC anode exhaust.

The *H-3* external heater it is used to reach the operating temperature of the SOFC when the RCR is operated at lower temperature than the SOFC. On the other side, the heat exchanger *HX-4* has been introduced before the external heater *H-4*, to preheat the ambient air entering the SOFC (*cathode in*) with the SOFC cathode outlet.

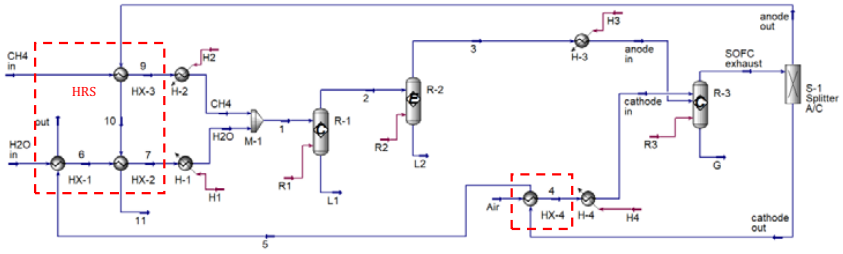


**Figure 8.** Heat recovery arrangement in the G2P mode.

## 3. Electrochemical model

The tuning of the r-SOC model is based on electrochemical data derived from a manufacturer's polarization curve, covering both the SOEC and SOFC operating regimes, confirmed also through experimental tests carried out in different operating points. All the details are given in the paragraphs below.

*3.1 Reversible Solid Oxide cell Design point*

The r-SOC data are based on a commercial stack (manufactured by SolydEra [16]) tested at CNR laboratories. In order to define the r-SOC operating points and the corresponding electrochemical performance, the experimental polarization curve (cell voltage-current density) reported in Figure 9 has been considered. In particular, experimental points of SOEC operation (i.e., negative values of current density) and of SOFC operation (positive current density) are shown, obtained for a temperature value equal to 700 °C. Starting from these experimental points, a fitting linear trend line has been used in the study to model the electrochemical behaviour of the r-SOC device.

In charging mode, the r-SOC has been considered operating in thermoneutral conditions (SOEC operating point, shown with the blue star in Figure 9). The cell thermoneutral potential ($V_{tn}$) [13] for the SOEC point can be calculated as:

$$V_{tn} = \Delta H°/nF \tag{10}$$

where $n$ is the number of electrons, $F$ [C/mol] is the Faraday constant, and $\Delta H°$ [kJ/kmol] is the specific enthalpy variation of the reaction.

On the other hand, in discharging mode (SOFC operation) the cell can work in different exothermic conditions depending on the selected operating point on the polarization curve. In this work, the SOFC design operating point (shown with the red star in Figure 9) has been selected to a given SOFC power output, equal to 1/3 of the SOEC input power setpoint, according to the reference commercial r-SOC stack nameplate data [16]. To find the operating point of the SOFC on the polarization curve, eq. (11) can be used:

$$rJ^2 - V_{OCV} \cdot J + P_{el}/(N \cdot A) = 0 \tag{11}$$

where, $r$ is the angular coefficient of the polarization linear fitting curve, $V_{OCV}$ is the experimental open circuit voltage [V] (intercept point of the y-axis in Figure 9, corresponding to a null value of

the current density), $P_{el}$ is the SOFC setpoint of electrical power produced by the stack [kW], $J$ is the current density [A/cm²], $N$ is the number of cells [-] and $A$ is the cell surface area [cm²].

The considered r-SOC (SOEC and SOFC) design set points are reported in Table 3 and in Figure 9 on the polarization curve, with the corresponding power density values.

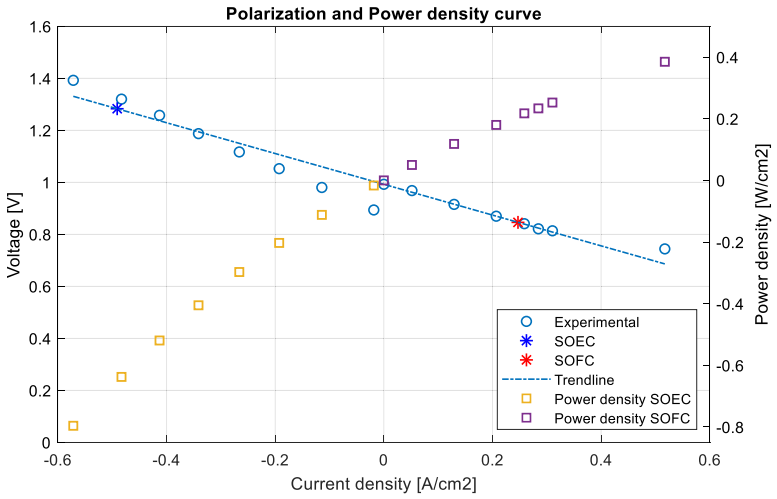


**Figure 9.** Cell polarization curve and power density of the r-SOC section.

**Table 3.** r-SOC section design set points and electrochemical operating data (at T=700°C).

| | Parameter | Value | Units |
|---|---|---|---|
| | Number of cells (N) | 70 | - |
| | Cell area (A) | 82 | cm² |
| | $V_{ocv}$ | 0.99 | V |
| | $\Delta H°$ | 247.52 | MJ/kmol |
| SOEC | $V_{tn}$ | 1.28 | V |
| | $J_{tn}$ | 0.49 | A/cm² |
| | $P_{tn}$ | 3.60 | kW |
| SOFC | $V$ | 0.85 | V |
| | $J$ | 0.25 | A/cm² |
| | $P_{el}$ | 1.20 | kW |

### *3.2. Off-design model of the Reversible Solid Oxide Cell*

In order to simulate the r-SOC and the whole system in part-load conditions, an off-design simplified modelling approach has been adopted.

The off-design of the r-SOC (in both the SOEC and SOFC mode) is based on the fitting function of the polarization curve. For a given part-load electric power value, the corresponding cell voltage value of interest ($V$) and the corresponding current density ($J$) can be calculated through the polarization curve of Figure 9. The electric power setpoint ($P_{el}$)[kW] is expressed by:

$$P_{el} = V \cdot J \cdot N \cdot A \quad (12)$$

The actual r-SOC inlet and outlet flow rates of reactants and products at part-load are calculated using the ASPEN thermodynamic model, by setting the off-design electric power, with the same approach described in [17] for SOEC. In particular, in P2G mode the SOEC inlet water flow is adjusted to match the setpoint of inlet electric power; in G2P mode, the methane inlet flow is adjusted to match the setpoint of SOFC electric power.

The off-design thermal power demand/production involved in the r-SOC operation can be also calculated. Specifically, for a given $V$ value, the voltage losses, $Q_p$ [kW], the Joule losses, $Q_j$ [kW], and the heat of reaction, $Q_r$ [kW], can be calculated, respectively, by the following expressions [13]:

$$Q_p = (V - V_{ocv}) \cdot J \cdot N \cdot A \quad (13)$$
$$Q_j = (V_{th} - V) \cdot J \cdot N \cdot A \quad (14)$$
$$Q_r = (V_{th} - V_{ocv}) \cdot J \cdot N \cdot A \quad (15)$$

In particular, the value $Q_j$ represents the net heat contribution that needs to be supplied to (or is delivered by) the r-SOC. This term is used to obtain the off-design r-SOC outlet temperature deviation, in comparison with the value in design conditions.

Concerning the RCR off-design, the methanation sections work at their optimum point, i.e., at the highest conversion rate, which corresponds to 550°C and 450°C for the high and medium temperature sections, respectively. Furthermore, the reformer off-design operating temperature is kept equal to 600°C.

In addition, the boundary conditions introduced in sections 2.1.1 for the design point (ratio of $O_2$ produced to $O_2$ in *Anode out* equal to 0.11) and 2.2.2 (Air/$H_2$ ratio equal to 9) are held constant; consequently, the flow rates of the *Sweep Air* (Figure 3) and *Air* (Figure 5) streams are changed as a function of $O_2$ and $H_2$ produced, respectively.

## 5. Performance parameters

In this study, different performance parameters are analysed to evaluate the potential of the P2P system in each mode. In particular, for the P2G system, the performance parameters taken into account are the electric-to-fuel efficiency (E2F) [-] (16) and the first law efficiency [-] (17), respectively defined as follows:

$$\eta_{E2F} = \frac{\dot{m}_{SNG} \cdot LHV_{SNG}}{P_{el,in}} \quad (16)$$

$$\eta_I = \frac{\dot{m}_{SNG} \cdot LHV_{SNG}}{P_{el,in} + Q_{in}} \quad (17)$$

where, $\dot{m}_{SNG}$ [kg/s] is the mass flow rate of produced synthetic natural gas (SNG), $LHV_{SNG}$ [kJ/kg] is the Lower Heating Value of the outlet SNG, $P_{el,in}$ [kW] is the SOEC input electric power and $Q_{in}$ [kW] is the entire amount of heat required by the system.

For the G2P system, the performance parameters taken into account are the fuel-to-electric efficiency (F2E) [-] (18) and the first law efficiency [-] (19), respectively defined as follows:

$$\eta_{F2E} = \frac{P_{el,out}}{\dot{m}_{CH4} \cdot LHV_{CH4}} \quad (18)$$

$$\eta_{I} = \frac{P_{el,out} + Q_{out}}{\dot{m}_{CH4} \cdot LHV_{CH4} + Q_{in}} \quad (19)$$

where, $\dot{m}_{CH4}$ [kg/s] is the mass flow of inlet $CH_4$ at the reformer section, $LHV_{CH4}$ [kJ/kg] is the Lower Heating Value of $CH_4$, $P_{el,out}$ [kW] is the SOFC output electric power and $Q_{out}$ [kW] is the amount of heat released by the SOFC. To evaluate the whole system performance in terms of electricity storage capability, the round-trip efficiency [-] (20) can be also considered:

$$\eta_{RT} = \eta_{E2F} \cdot \eta_{F2E} \quad (20)$$

## 6 Results and discussion

In this section, the results obtained by the analysis of the r-SOC device (Figure 3 and Figure 5), operating both in design and in off-design, and the study of the thermal synergy of the P2P system are analyzed (Figure 6 and Figure 7). Firstly, the results of the off-design operation are discussed, by showing the performance indicators versus the actual input/output electric power. Secondly, a comparison of the system performance, with and without internal heat recovery, is carried out.

### *6.1 Off-design of reversible Solid Oxide Cell operation results*

The r-SOC off-design thermal and electric power values are shown in Figure 10 versus the cell current density.

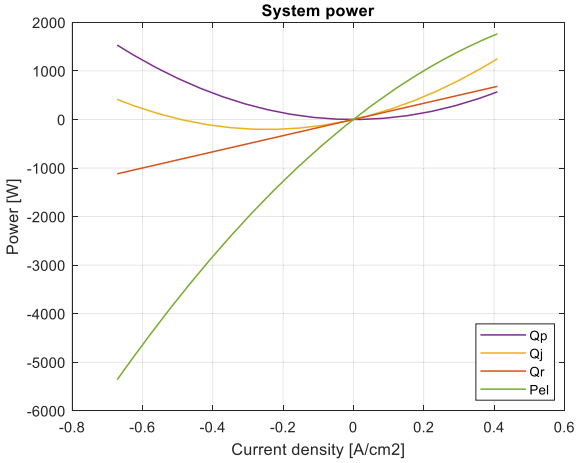


**Figure 10.** Power variation terms as a function of the cell current density.

In particular, it can be seen that $Q_p$ is always positive, while $Q_r$ is negative during operation in SOEC mode and positive in SOFC mode. The $Q_j$ term varies depending on whether the SOEC is working in exothermic or endothermic mode; indeed, it can be seen that at the thermoneutral point $Q_j$ is zero, while in operation as SOFC it is always positive. Figure 10 also illustrates the

power required by the system and the corresponding thermal contribution depending on the type of operation described above.

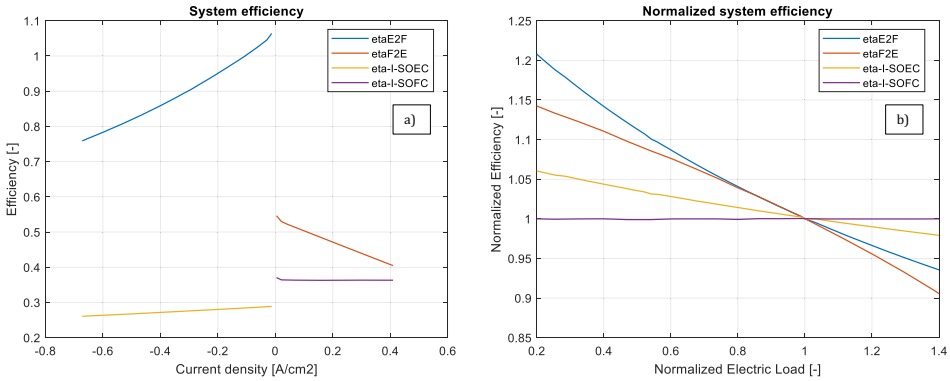


**Figure 11.** Efficiency variation as a function of a) current density and b) normalized electric load.

Figure 11a shows the trend of the efficiency terms of the system versus the cell current density, while Figure 11b shows a map of efficiency versus the electric power load, in both P2G and G2P modes. It can be seen that the E2F and F2E efficiency values undergo a significant increase at part-load conditions (more than 10% of $\eta_{E2F}$ increase occurs at 50% of the SOEC nominal input load, and almost 10% of $\eta_{F2E}$ increase when the SOFC output load is reduced to 50%). In contrast, the SOFC-related first-law efficiency is almost constant as the load changes, while the SOEC first-law efficiency tents to increase at part-load (less than 5% of $\eta_I$ increase with a 50% load reduction.

*6.2 P2P system's results at design conditions*

The power demand contributions calculated for the two analysed system configurations (at the design point, with and without heat recovery), operating in P2G and G2P, are summarized in Table 4 and 5, respectively, while Table 6 shows the resulting efficiency terms obtained assuming design conditions for both the P2G and G2P modes. In the P2G mode, the external heat required (mainly in *H-1* and *H-2*) is significantly reduced by the HRS, from 1.01 kW to 0.15 kW for *H-1*, and from 5.91 kW to 1.24 kW for *H-2*.

In the charge phase, the E2F efficiency is characterized by a high value, 82%, while in the discharge phase the F2E efficiency drops to around 46%. Results allow to demonstrate the key role of the HRS: indeed, without heat recovery, the first-law efficiency is less than 40%, both for the P2G and G2P systems. In case of thermal recovery, both the P2G and G2P first law efficiency values in design conditions are above 50%.

**Table 4.** Comparison of P2G system parameters with and without heat recovery for the system operating at design point.

| | Components | External Heat [kW] | Electrical Power [kW] | Heat Recovery [kW] |
|---|---|---|---|---|
| No Heat Recovery (Figure 3) | *H-1* | 1.01 | - | - |
| | *H-2* | 5.91 | - | - |
| | *H-3* | $2.09e^{-2}$ | - | - |
| | *C-1* | $5.38e^{-2}$ | - | - |
| | *C-2* | 0.49 | - | - |
| | *R-1* | - | 3.60 | - |
| Heat Recovery (Figure 6) | *H-1* | 0.15 | - | - |
| | *H-2* | 1.24 | - | - |
| | *H-3* | $5.48e^{-2}$ | - | - |
| | *C-1* | 0 | - | - |
| | *C-2* | 0.35 | - | - |
| | *R-1* | - | 3.60 | - |
| | *HX-1* | - | - | 4.67 |
| | *HX-2* | - | - | 0.64 |
| | *HX-3* | - | - | 0.14 |
| | *HX-4* | | | 0.09 |
| | *HX-5* | - | - | 0.05 |

**Table 5.** Comparison of G2P system parameters with and without heat recovery for the system operating at design point.

| | Components | External Heat [kW] | Electrical Power [kW] | Heat Recovery [kW] |
|---|---|---|---|---|
| No Heat Recovery (Figure 5) | *H-1* | 0.64 | - | - |
| | *H-2* | $9.69e^{-2}$ | - | - |
| | *H-3* | $6.70e^{-2}$ | - | - |
| | *H-4* | 1.54 | - | - |
| | *R-3* | 0.62 | 1.20 | - |
| Heat Recovery (Figure 7) | *H-1* | $1.17e^{-2}$ | - | - |
| | *H-2* | 0 | - | - |
| | *H-3* | $6.70e^{-2}$ | - | - |
| | *H-4* | 0.58 | - | - |
| | *R-3* | 0.62 | 1.20 | - |
| | *HX-1* | - | - | 0.46 |
| | *HX-2* | - | - | 0.17 |
| | *HX-3* | - | - | 0.10 |
| | *HX-4* | - | - | 0.97 |

**Table 6.** performance indicators of the P2P system for the system operating at design point.

| | Efficiency | Value |
|---|---|---|
| | $\eta_{E2F}$ | 0.82 |
| | $\eta_{F2E}$ | 0.46 |
| | $\eta_{RT}$ | 0.38 |
| No Heat Recovery | $\eta_{I,P2G}$ | 0.27 |
| | $\eta_{I,G2P}$ | 0.36 |
| Heat Recovery | $\eta_{I,P2G}$ | 0.55 |
| | $\eta_{I,G2P}$ | 0.55 |

## 7 Conclusion

In this paper, an innovative P2P system for green electricity storage is proposed and analyzed. The system combines a reversible Solid Oxide Cell stack and a reversible chemical reactor acting as methanator/reformer. The model of the integrated system, developed in Aspen HYSYS™ environment, is based on experimental data of yield for the main components, obtained at lab-scale.

An off-design analysis of the r-SOC device was performed, including the effect of the thermal powers involved in the system. Electric-to-fuel, fuel-to-electric, and first-law efficiencies were evaluated at part-load in both charging and discharging modes. Moving out of the thermoneutral point (SOEC design point), significant efficiency deviations can occur, up to +30% at part-load and -15% in overload conditions.

Concerning the P2P system performance, both a simple and an optimized configuration, considering internal heat recovery, have been analyzed, demonstrating the achievable benefits in terms of first-law efficiency: an increase from 27% to 55% is seen for the P2G system first-law efficiency and from 36% to 55% for the G2P system first-law efficiency.

A further future analysis is to use the anode stream of the SOFC containing water to power the reformer, in order to reduce the external heat input for water preheating.

## References

[1] Jalili M *et al* 2023 Electrolyzer cell-methanation/Sabatier reactors integration for power-to-gas energy storage: Thermo-economic analysis and multi-objective optimization *Applied Energy* **329** 120268
[2] Cinti G *et al* 2016 Integration of Solid Oxide Electrolyzer and Fischer-Tropsch: A sustainable pathway for synthetic fuel *Applied Energy* **162** pp 308–320
[3] Venkataraman V *et al* 2019 Reversible solid oxide systems for energy and chemical applications – Review & perspectives *Journal of Energy Storage* **24** 100782
[4] Giglio E *et al* 2015 Synthetic natural gas via integrated high-temperature electrolysis and methanation: Part I—Energy performance *Journal of Energy Storage* **1** pp 22–37
[5] Fujiwara N *et al* 2020 Power-to-gas systems utilizing methanation reaction in solid oxide electrolysis cell cathodes: a model-based study *Sustainable Energy Fuels* **4** 2691
[6] Paulina Pianko-Oprych and Palus M 2017 Simulation of SOFCs based power generation system using Aspen. *Polish Journal of Chemical Technology* **19** 4
[7] Hauck M *et al* 2017 Simulation of a reversible SOFC with Aspen Plus *ScienceDirect* **42** pp 10329–10340

[8] Chen B *et al* 2019 Integration of reversible solid oxide cells with methane synthesis (ReSOC-MS) in grid stabilization: A dynamic investigation *Applied Energy* **250** pp 558–567
[9] Ancona M A *et al* 2019 Thermal integration of a high-temperature co-electrolyzer and experimental methanator for Power-to-Gas energy storage system *Energy Conversion and Management* **186** pp 140–155, https://doi.org/10.1016/j.enconman.2019.02.057
[10] AspenTech *AspenHysys* https://www.aspentech.com/en/products/engineering/aspen-hysys
[11] Jolaoso L A *et al* 2023 Operational and scaling-up barriers of SOEC and mitigation strategies to boost H2 production- a comprehensive review *Hydrogen Energy* **48** pp 33017–33041
[12] AlZahrani A A and Dincer I 2017 Thermodynamic and electrochemical analyses of a solid oxide electrolyzer for hydrogen production *Hydrogen Energy* **42** pp 21404 - 21413
[13] Penchini D 2014 Theoretical study and performance evaluation of hydrogen production by 200 W solid oxide electrolyzer stack *Hydrogen Energy* **39** pp 9457-9466
[14] Italiano C *et al* 2022 Silicon carbide and alumina open-cell foams activated by Ni/CeO2-ZrO2 catalyst for CO2 methanation in a heat-exchanger reactor *Chemical Engineering Journal* **434** 134685
[15] Zeng Z *et al* 2020 A review of heat transfer and thermal management methods for temperature gradient reduction in solid oxide fuel cell (SOFC) stacks *Applied Energy* **280** 115899
[16] SolydEra *G8 Stack Technical data* https://www.solydera.com/it/
[17] Ancona M.A. *et al* 2020 Numerical prediction of off-design performance for a Power-to-Gas system coupled with renewables *Energy Conversion and Management* **210** 112702, https://doi.org/10.1016/j.enconman.2020.112702